Selective Electrochemical Nitrogen Reduction Driven by Hydrogen Bond Interactions at Metal−Ionic Liquid Interfaces

Manuel A. Ortuño,*,[†] Oldamur Hollóczki,[‡] Barbara Kirchner,[‡] and Núria López*,[†]

[†]Institute of Chemical Research of Catalonia (ICIQ) and Barcelona Institute of Science and Technology (BIST), Av. Països Catalans 16, 43007 Tarragona, Spain

[‡]Institut für Physikalische und Theoretische, Universität Bonn, Mulliken Center for Theoretical Chemistry, Beringstrasse 4−6, 53115 Bonn, Germany

S *Supporting Information*

ABSTRACT: Increasing the activity of the nitrogen reduction reaction while slowing the detrimental hydrogen evolution reaction is a key challenge in current electrocatalysis to provide a sustainable route to ammonia. Recently, nanoparticles in ionic liquid (IL) environments have been found to boost the selectivity of electrochemical synthesis of ammonia from dinitrogen at room temperature. Here, we use for the first time a fully atomistic representation of metal−IL interfaces at the density functional theory level to understand experimental evidence, with particular focus on the rate and selectivity determining formation of N_2H intermediates compared to hydrogen evolution. We find that decorating the metal surface with fluorinated ILs creates specific H-bond interactions between Ru−N_2H and IL anions, stabilizing this intermediate and thus driving the selectivity of the electrochemical process.
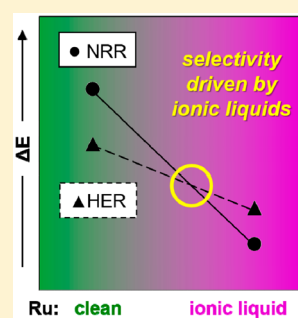
Ammonia synthesis, one of the most important processes in the chemical industry, keeps the supply of fertilizers and related N-containing chemicals worldwide. The Haber−Bosch process, which involves the thermally driven hydrogenation of N_2 under harsh pressure and temperature conditions, produces 500 million tons of NH_3 per year and consumes ca. 1% of the global energy.[1] Transition from Haber−Bosch to less energy-demanding processes is a major goal in chemistry.[2,3]

Mimicking the gentle reaction conditions found in enzymes, electrocatalysis is a promising alternative to achieve the nitrogen reduction reaction (NRR) at low temperature.[4−6] The challenge is promoting the NRR while shutting down the competing hydrogen evolution reaction (HER) that reduces the efficiency of the process.[7] However, the rational design of new only metal-based catalysts with enhanced selectivity is limited by how the stabilities of certain intermediates are dependent on each other, in other words, by linear scaling relationships.[8,9]

Experimental efforts have boosted Faradaic efficiencies by working in a molten hydroxide suspension at high temperature[10] and supporting Au nanoparticles on CeO$_x$−reduced graphite oxide.[11] Quite recently, MacFarlane and coworkers reported Fe-based catalysts with a Faradaic efficiency of 32%[12] and 60%[13] when using fluorinated ionic liquids (ILs). Besides the relatively higher solubility of N_2 in ILs,[14] the specific role of ILs on the selective NRR is not fully understood. To shed light into these features, we turn to theoretical methods.[15]

Herein, we employed density functional theory (DFT) to gain mechanistic insight on IL-decorated metal surfaces[16] for the electrochemical reduction of N_2 to NH_3 (Figure 1a). Such metal−IL interfaces have the potential to circumvent linear scaling relationships, which opens the path to enhanced NRR
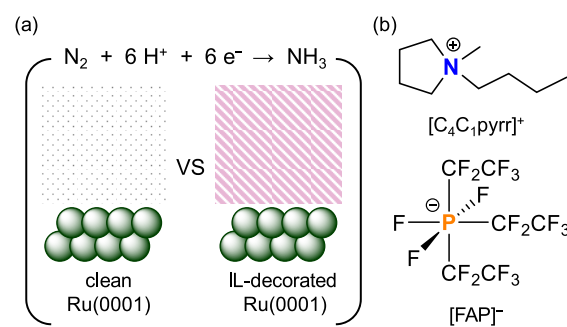
Figure 1. (a) Ru-catalyzed electrochemical nitrogen reduction reaction on clean (dotted square) and IL-decorated (striped square) surfaces. (b) N-Butyl-N-methylpyrrolidinium $[C_4C_1pyrr]^+$ and tris-(perfluoroethyl)-trifluorophosphate $[FAP]^-$ under study.

selectivity. We modeled a Ru-based catalyst, as studied in literature,[17] and the IL $[C_4C_1pyrr][FAP]$ (Figure 1b), as reported experimentally.[13] Computational studies on bulk ILs have been extensively reported,[18] but due to its complexity, less attention has been paid to their interface with solids.[19,20] Pádua and coworkers[21] parametrized metal−IL interactions to study the solvation of Ru nanoparticles, and Heinz et al.[22] performed classical molecular dynamics (MD) simulations on Au−IL structures. To the best of our knowledge, this is the first fully atomistic study of a bulk IL on a transition metal surface at DFT level that directly addresses reactivity.

First, to evaluate the dynamic behavior of the fluorinated IL at hand, we described the liquid phase of the pure IL,[23] N_2@ IL, and NH_3@IL by means of classical MD simulations. We used a cubic box with 240 IL pairs to model the bulk phase (Figure 2a). For N_2@IL and NH_3@IL, we included one N_2 or
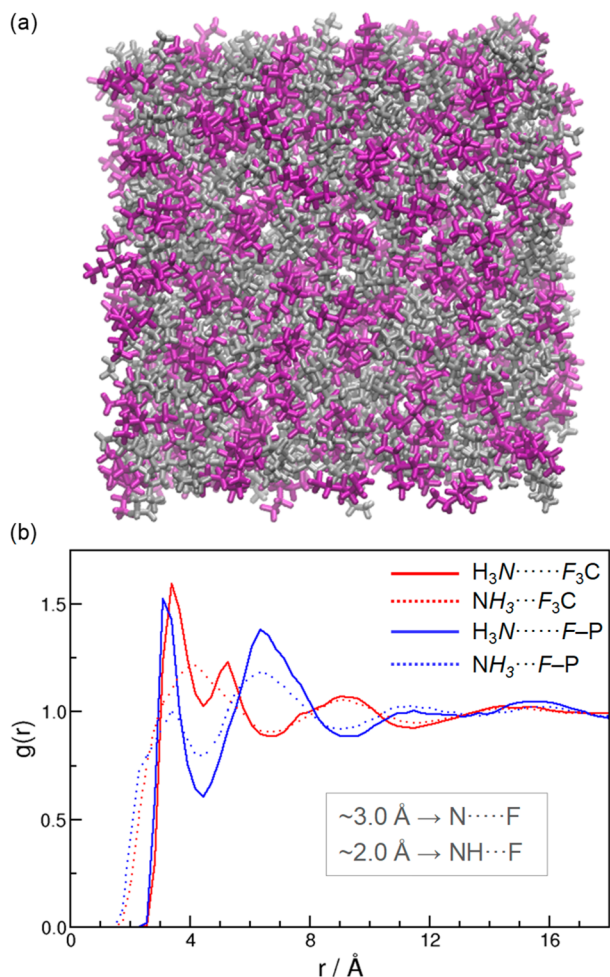

Figure 2. Classical MD simulations. (a) Cubic box containing 240 IL pairs (cations in gray, anions in purple) and (b) corresponding RDFs for the NH_3@IL simulation, highlighting contacts between the H atoms of NH_3 and the F atoms of $[FAP]^-$.

one NH_3 molecule per simulation box, respectively. Radial distribution function (RDF) data, which show probable atom−atom distances, can be consulted in Figures S2−4 for all three simulations. RDF data for the N_2@IL simulation (Figure S3) show significant contact between N_2 and the methyl C atom of the butyl chain of $[C_4C_1pyrr]^+$, suggesting that N_2 might be mainly in the nonpolar microphase. The most relevant RDF data for the NH_3@IL simulation are summarized in Figure 2b. At ~3 Å, one can observe interplays between the N atom of NH_3 and (i) the F atoms of the CF_3 groups ($F−CF_2$) in $[FAP]^-$ anions (solid red line) and (ii) the F atoms directly attached to P ($F−P$) in $[FAP]^-$ anions (solid blue line). Concurrently, some interactions can be detected starting at ~2 Å between the H atoms of NH_3 and $F−CF_2$ and $F−P$ atoms (dashed red and blue lines, respectively). The occasional close approach of the H and F atoms results in a shoulder on the RDFs and points to the possibility of a weak H-bond interaction between NH_3 and $[FAP]^-$. The interactions

between the N atom and the inner $F−CF$ atoms are less marked than those involving the more accessible $F−CF_2$ and $F−P$ atoms (Figure S4). Additional RDF data from classical and first-principles MD simulations with 24 IL pairs can be consulted in Figures S5−6.

Next, we explored the interface between the Ru catalyst and the IL. For that purpose, we designed a 3-layer p(6 × 6) Ru(0001) slab with 8 IL pairs equilibrated through classical and first-principles MD simulations. The use of isolated IL pairs would not capture the bulk effect of the liquid; likewise, continuum methods would not describe explicit interactions between solute and solvent. The aim here is to describe the IL as a bulk liquid rather than as isolated pair clusters. The final structure after equilibration is shown in Figure 3a. Close
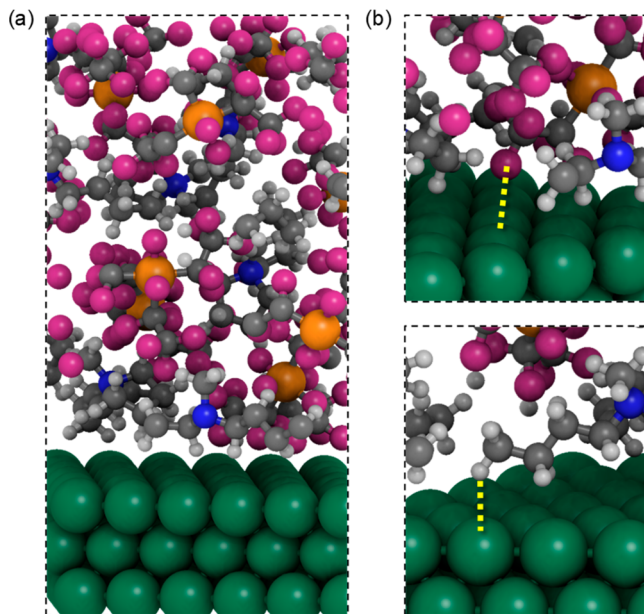

Figure 3. First-principles MD simulations. (a) Repeating unit cell of the interface formed by a 3-layer p(6 × 6) Ru(0001) slab with 8 IL pairs (548 atoms) and (b) zoom-in insets highlighting Ru···F (top) and Ru···H (bottom) close contacts. Legend: Ru (green), P (orange), F (pink), N (blue), C (gray), H (white).

contacts between the Ru surface and the $F−CF_2$ group in $[FAP]^-$ (Ru···F distance of 3.026 Å) and the $H−CH_2$ group of the butyl chain in $[C_4C_1pyrr]^+$ (Ru···H distance of 2.363 Å) are depicted in Figure 3b.

With an atomistic representation of the clean metal and the metal−IL interface at hand, we next evaluated the potential energy surface of the nitrogen reduction and hydrogen evolution reactions at DFT level. Species involving the clean surface are denoted with **A−E**. The corresponding IL-decorated counterparts follow the same nomenclature and add the prefix IL. Due to the rich chemical composition of the interface (Figure 3b), we found several configurations for each intermediate, but only the most stable ones are reported here. The explicit representation of the solvent on clean metal surfaces[24] is out of the scope of the present work, which rather focuses on the selectivity induced by ILs.

Guided by previous computational studies on Ru catalysts,[8,25−27] we focused on the adsorption of N_2 and formation of the N_2H intermediate, a key rate- and selectivity-determining step (additional intermediates can be consulted in Table S1) and also computed the competitive hydrogen

evolution to address selectivity (Figure 4a). Figure 4b displays the relative electronic energies of key intermediates during
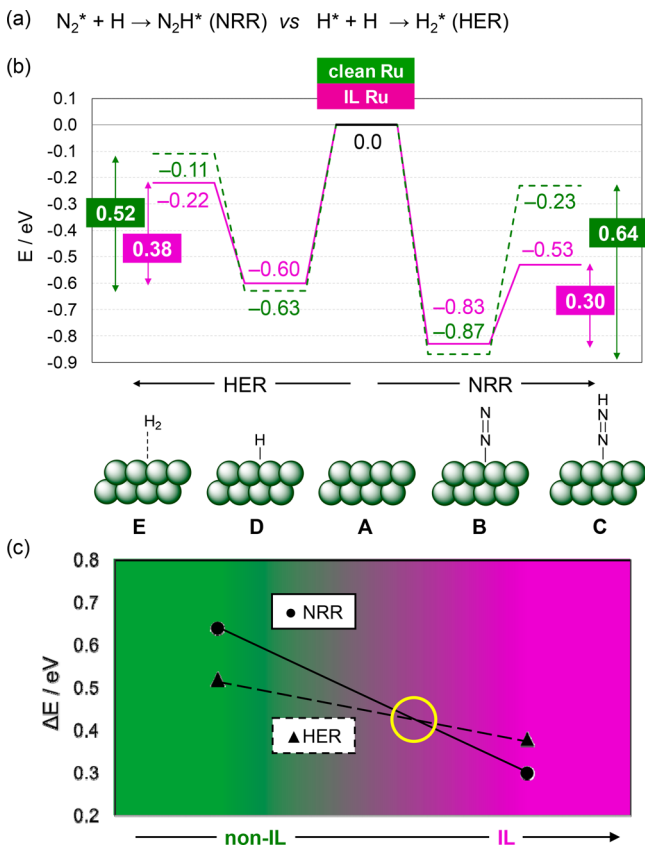

Figure 4. (a) Rate and selectivity determining step comparison studied herein and (b) corresponding reaction energy profiles of such intermediates during NRR (right) and HER (left) for clean (dashed green line) and IL-decorated (solid purple line) Ru surfaces. (c) Relative energy differences for NRR (circles) and HER (triangles) according to the absence (green) and presence (purple) of IL. The change of selectivity from HER to NRR is indicated with a yellow circle. Lines (solid for NRR, dashed for HER) serve as a guide to the eye.

NRR (right side) and HER (left side). On the one hand, the dashed green line shows the energy values for the clean Ru surfaces. The end-on adsorption of N_2 on **A** giving rise to **B** is exothermic by 0.87 eV (the side-on adsorption is only 0.23 eV downhill). Subsequent formation of the N_2H intermediate **C** demands 0.64 eV above **B**. Regarding HER, the reaction from **D**, adsorbed H, to **E**, physisorbed H_2, requires 0.52 eV. The lower relative energy of HER (0.52 eV) compared to that of NRR (0.64 eV) explains the low selectivity toward ammonia observed for pure metal catalysts. On the other hand, the solid purple line shows the energy values for the IL-decorated Ru surfaces. The end-on adsorption of N_2 on IL-**A** to form IL-**B** is also exothermic by 0.83 eV (the side-on adsorption is only 0.20 eV downhill), suggesting that the IL surroundings play a small role at this stage. However, the formation of the N_2H intermediate IL-**C** is significantly favored, requiring only 0.30 eV comapred to 0.64 eV for the clean surface. As for HER, the H_2 formation from IL-**D** to IL-**E** demands 0.38 eV. This value is lower than that for HER with the clean surface, 0.52 eV, but slightly higher than that for NRR with the IL-decorated surface, 0.30 eV. These results show that the IL environment

increases both the activity (by stabilizing IL-**C** compared to **C**) and selectivity (by stabilizing IL-**C** compared to IL-**E**). Such effect is better displayed in Figure 4c, which represents how the selectivity to HER for the non-IL system (left) switches to NRR in the presence of IL (right). The effect of the IL on selectivity remains the same when considering zero point vibrational energy corrections and Gibbs energies (Table S3).

The above-mentioned results can be explained by looking at the atomic structure of the N_2H intermediate in Figure 5a.
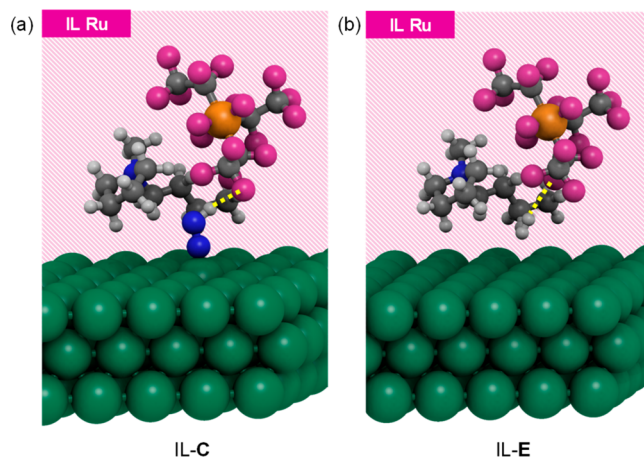

Figure 5. DFT-optimized structures of (a) the N_2H intermediate, IL-**C**, and (b) the H_2 intermediate, IL-**E**, both including an IL configuration coming from the metal−IL MD simulations. Selected ILs are omitted for clarity. The yellow dashed lines highlight H···F interactions. Legend: Ru (green), P (orange), F (pink), N (blue), C (gray), H (white).

Compared to the Ru-only surface **C**, IL-**C** exhibits a clear interaction between the N_2H group and the $F−CF_2$ atom in $[FAP]^-$. The H···F and N···F distances of 1.865 and 2.871 Å, respectively, evoke the patterns found in the liquid NH_3@IL simulation (Figure 2b). Likewise, similar contacts might also be at work on N_2H_x species[28] or dissociative mechanisms involving NH_x intermediates.[25−27] Binding energies of ca. 0.1 eV have been estimated for related contacts involving CH_3OH and CH_3CF_3.[29] Our relative ΔE of 0.34 eV between **B** and **C** (0.64 eV) and IL-**B** and IL-**C** (0.30 eV) suggests that this interaction alone might not be responsible for the stabilization and that the inherently charged bulk IL environment has an additional electrostatic effect[30−32] and should not be ignored in the modeling. As for the competing HER, the H_2 intermediate IL-**E** is shown in Figure 5b. The interaction between the nonpolar H_2 and F atoms is weaker (H···F distance of 2.471 Å), and thus, the stabilization is less marked compared to N_2H species. Overall, H···F interactions in IL-containing NRR intermediates boost the selectivity of the process, in line with recent experiments.[13]

With respect to the role of reactant water, it has been shown that (i) the OH groups of hexafluoroisopropanol cluster together, forming polar domains, and are separated from the fluorine-based groups,[33] and (ii) NH-based species with a free lone pair interact with water as H-bond acceptors rather than H-bond donors. This suggests that N_2H···F interactions, in which N_2H acts as H-bond donor (Figure 5a), will be probably not disturbed. In agreement with this discussion, experiments show that the concentration of water (from 20 to 250 ppm) did not strongly impact the selectivity of the reaction.[13]

In conclusion, we followed an elaborated computational protocol to model metal−ionic liquid interfaces at the DFT level. Particularly, we designed a Ru(0001) surface in contact with 8 pairs of $[C_4C_1pyrr][FAP]$. We used the resulting model to study the key rate and selectivity determining N_2H intermediate in the NRR compared to the HER involved in the electrochemical synthesis of ammonia at room temperature. Our results indicate that interactions between Ru−N_2H species and F atoms of the $[FAP]^-$ anion increase activity and boost selectivity toward ammonia. Such fully atomistic computational approach holds promise to unravel new mechanistic features and guide the rational design of novel electrocatalytic interfaces for ammonia synthesis.

■ ASSOCIATED CONTENT

Ⓢ Supporting Information

The Supporting Information is available free of charge on the

Computational details, radial distribution functions, intermediates, energies (PDF)

Cartesian coordinates (XYZ)

■ AUTHOR INFORMATION

Corresponding Authors
*E-mail: mortuno@iciq.es.
*E-mail: nlopez@iciq.es.
ORCID Ⓞ
Manuel A. Ortuño: 0000-0002-6175-3941
Oldamur Hollóczki: 0000-0003-3105-7176
Barbara Kirchner: 0000-0001-8843-7132
Núria López: 0000-0001-9150-5941
Notes
The authors declare no competing financial interest.

■ ACKNOWLEDGMENTS

■ REFERENCES

(1) Erisman, J. W.; Sutton, M. A.; Galloway, J.; Klimont, Z.; Winiwarter, W. How a Century of Ammonia Synthesis Changed the World. *Nat. Geosci.* **2008**, *1*, 636−639.

(2) Foster, S. L.; Perez Bakovic, S. I.; Duda, R. D.; Maheshwari, S.; Milton, R. D.; Minteer, S. D.; Janik, M. J.; Renner, J. N.; Greenlee, L. F. Catalysts for Nitrogen Reduction to Ammonia. *Nat. Catal.* **2018**, *1*, 490−500.

(3) Martín, A. J.; Shinagawa, T.; Pérez-Ramírez, J. Electrocatalytic Reduction of Nitrogen: From Haber-Bosch to Ammonia Artificial Leaf. *Chem.* **2018**, DOI: 10.1016/j.chempr.2018.10.010.

(4) Guo, C.; Ran, J.; Vasileff, A.; Qiao, S.-Z. Rational Design of Electrocatalysts and Photo(electro)catalysts for Nitrogen Reduction to Ammonia (NH_3) under Ambient Conditions. *Energy Environ. Sci.* **2018**, *11*, 45−56.

(5) Deng, J.; Iñiguez, J. A.; Liu, C. Electrocatalytic Nitrogen Reduction at Low Temperature. *Joule* **2018**, *2*, 846−856.

(6) Cui, X.; Tang, C.; Zhang, Q. A Review of Electrocatalytic Reduction of Dinitrogen to Ammonia under Ambient Conditions. *Adv. Energy Mater.* **2018**, *8*, 1800369.

(7) Singh, A. R.; Rohr, B. A.; Schwalbe, J. A.; Cargnello, M.; Chan, K.; Jaramillo, T. F.; Chorkendorff, I.; Nørskov, J. K. Electrochemical Ammonia Synthesis—The Selectivity Challenge. *ACS Catal.* **2017**, *7*, 706−709.

(8) Montoya, J. H.; Tsai, C.; Vojvodic, A.; Nørskov, J. K. The Challenge of Electrochemical Ammonia Synthesis: A New Perspective on the Role of Nitrogen Scaling Relations. *ChemSusChem* **2015**, *8*, 2180−2186.

(9) Singh, A. R.; Montoya, J. H.; Rohr, B. A.; Tsai, C.; Vojvodic, A.; Nørskov, J. K. Computational Design of Active Site Structures with Improved Transition-State Scaling for Ammonia Synthesis. *ACS Catal.* **2018**, *8*, 4017−4024.

(10) Licht, S.; Cui, B.; Wang, B.; Li, F.-F.; Lau, J.; Liu, S. Ammonia Synthesis by N_2 and Steam Electrolysis in Molten Hydroxide Suspensions of Nanoscale Fe_2O_3. *Science* **2014**, *345*, 637−640.

(11) Li, S.-J.; Bao, D.; Shi, M.-M.; Wulan, B.-R.; Yan, J.-M.; Jiang, Q. Amorphizing of Au Nanoparticles by CeO_x−RGO Hybrid Support towards Highly Efficient Electrocatalyst for N_2 Reduction under Ambient Conditions. *Adv. Mater.* **2017**, *29*, 1700001.

(12) Suryanto, B. H. R.; Kang, C. S. M.; Wang, D.; Xiao, C.; Zhou, F.; Azofra, L. M.; Cavallo, L.; Zhang, X.; MacFarlane, D. R. Rational Electrode−Electrolyte Design for Efficient Ammonia Electrosynthesis under Ambient Conditions. *ACS Energy Lett.* **2018**, *3*, 1219−1224.

(13) Zhou, F.; Azofra, L. M.; Ali, M.; Kar, M.; Simonov, A. N.; McDonnell-Worth, C.; Sun, C.; Zhang, X.; MacFarlane, D. R. Electrosynthesis of Ammonia from Nitrogen at Ambient Temperature and Pressure in Ionic Liquids. *Energy Environ. Sci.* **2017**, *10*, 2516−2520.

(14) Stevanovic, S.; Costa Gomes, M. F. Solubility of Carbon Dioxide, Nitrous Oxide, Ethane, and Nitrogen in 1-Butyl-1-methylpyrrolidinium and Trihexyl(tetradecyl)phosphonium Tris-(pentafluoroethyl)-trifluorophosphate (eFAP) Ionic Liquids. *J. Chem. Thermodyn.* **2013**, *59*, 65−71.

(15) Honkala, K.; Hellman, A.; Remediakis, I. N.; Logadottir, A.; Carlsson, A.; Dahl, S.; Christensen, C. H.; Nørskov, J. K. Ammonia Synthesis from First-Principles Calculations. *Science* **2005**, *307*, 555−558.

(16) Rotenberg, B.; Salanne, M. Structural Transitions at Ionic Liquid Interfaces. *J. Phys. Chem. Lett.* **2015**, *6*, 4978−4985.

(17) Hellman, A.; Honkala, K.; Remediakis, I. N.; Logadóttir, A.; Carlsson, A.; Dahl, S.; Christensen, C. H.; Nørskov, J. K. Ammonia Synthesis and Decomposition on a Ru-Based Catalyst Modeled by First-Principles. *Surf. Sci.* **2009**, *603*, 1731−1739.

(18) Kirchner, B.; Hollóczki, O.; Canongia Lopes, J. N.; Pádua, A. A. H. Multiresolution Calculation of Ionic Liquids. *WIREs Comput. Mol. Sci.* **2015**, *5*, 202−214.

(19) Buchner, F.; Forster-Tonigold, K.; Bozorgchenani, M.; Gross, A.; Behm, R. J. Interaction of a Self-Assembled Ionic Liquid Layer with Graphite(0001): A Combined Experimental and Theoretical Study. *J. Phys. Chem. Lett.* **2016**, *7*, 226−233.

(20) Weber, H.; Kirchner, B. Ionic Liquid Induced Band Shift of Titanium Dioxide. *ChemSusChem* **2016**, *9*, 2505−2514.

(21) Pensado, A. S.; Pádua, A. A. H. Solvation and Stabilization of Metallic Nanoparticles in Ionic Liquids. *Angew. Chem., Int. Ed.* **2011**, *50*, 8683−8687.

(22) Jha, K. C.; Liu, H.; Bockstaller, M. R.; Heinz, H. Facet Recognition and Molecular Ordering of Ionic Liquids on Metal Surfaces. *J. Phys. Chem. C* **2013**, *117*, 25969−25981.

(23) Paredes, X.; Fernández, J.; Pádua, A. A. H.; Malfreyt, P.; Malberg, F.; Kirchner, B.; Pensado, A. S. Bulk and Liquid−Vapor Interface of Pyrrolidinium-Based Ionic Liquids: A Molecular Simulation Study. *J. Phys. Chem. B* **2014**, *118*, 731−742.

(24) Bellarosa, L.; García-Muelas, R.; Revilla-Lopez, G.; Lopez, N. Diversity at the Water−Metal Interface: Metal, Water Thickness, and Confinement Effects. *ACS Cent. Sci.* **2016**, *2*, 109−116.

(25) Skulason, E.; Bligaard, T.; Gudmundsdottir, S.; Studt, F.; Rossmeisl, J.; Abild-Pedersen, F.; Vegge, T.; Jonsson, H.; Nørskov, J. K. A Theoretical Evaluation of Possible Transition Metal Electro-catalysts for N_2 Reduction. *Phys. Chem. Chem. Phys.* **2012**, *14*, 1235−1245.

(26) Back, S.; Jung, Y. On the Mechanism of Electrochemical Ammonia Synthesis on the Ru Catalyst. *Phys. Chem. Chem. Phys.* **2016**, *18*, 9161−9166.

(27) Wang, D.; Azofra, L. M.; Harb, M.; Cavallo, L.; Zhang, X.; Suryanto, B. H. R.; MacFarlane, D. R. Energy-Efficient Nitrogen Reduction to Ammonia at Low Overpotential in Aqueous Electrolyte under Ambient Conditions. *ChemSusChem* **2018**, *11*, 3416−3422.

(28) Yao, Y.; Zhu, S.; Wang, H.; Li, H.; Shao, M. A Spectroscopic Study on the Nitrogen Electrochemical Reduction Reaction on Gold and Platinum Surfaces. *J. Am. Chem. Soc.* **2018**, *140*, 1496−1501.

(29) Dalvit, C.; Invernizzi, C.; Vulpetti, A. Fluorine as a Hydrogen-Bond Acceptor: Experimental Evidence and Computational Calculations. *Chem. - Eur. J.* **2014**, *20*, 11058−11068.

(30) Choksi, T.; Majumdar, P.; Greeley, J. P. Electrostatic Origins of Linear Scaling Relationships at Bifunctional Metal/Oxide Interfaces: A Case Study of Au Nanoparticles on Doped MgO Substrates. *Angew. Chem., Int. Ed.* **2018**, *57*, 15410−15414.

(31) Aragonés, A. C.; Haworth, N. L.; Darwish, N.; Ciampi, S.; Bloomfield, N. J.; Wallace, G. G.; Diez-Perez, I.; Coote, M. L. Electrostatic Catalysis of a Diels−Alder Reaction. *Nature* **2016**, *531*, 88−91.

(32) Zhang, L.; Vogel, Y. B.; Noble, B. B.; Gonçales, V. R.; Darwish, N.; Le Brun, A.; Gooding, J. J.; Wallace, G. G.; Coote, M. L.; Ciampi, S. TEMPO Monolayers on Si(100) Electrodes: Electrostatic Effects by the Electrolyte and Semiconductor Space-Charge on the Electroactivity of a Persistent Radical. *J. Am. Chem. Soc.* **2016**, *138*, 9611−9619.

(33) Hollóczki, O.; Berkessel, A.; Mars, J.; Mezger, M.; Wiebe, A.; Waldvogel, S. R.; Kirchner, B. The Catalytic Effect of Fluoroalcohol Mixtures Depends on Domain Formation. *ACS Catal.* **2017**, *7*, 1846−1852.